

A comprehensive evaluation of the potential binding poses of fentanyl and its analogs
at the μ -opioid receptor

Bing Xie¹, Alexander Goldberg¹, Lei Shi^{1,*}

¹Computational Chemistry and Molecular Biophysics Section, Molecular Targets and Medications
Discovery Branch, National Institute on Drug Abuse – Intramural Research Program, National
Institutes of Health, Baltimore, MD 21224, USA

*corresponding author: lei.shi2@nih.gov

Abstract

Fentanyl and its analogs are selective agonists of the μ -opioid receptor (MOR). Among novel synthetic opioids (NSOs), they dominate the recreational drug market and are the main culprits for the opioid crisis, which has been exacerbated by the COVID-19 pandemic. By taking advantage of the crystal structures of the MOR, several groups have investigated the binding mechanism of fentanyl, but have not reached a consensus, in terms of both the binding orientation and the fentanyl conformation. Thus, the binding mechanism of fentanyl at the MOR remains an unsolved and challenging question. Here, we carried out a systematic computational study to investigate the preferred fentanyl conformations, and how these conformations are being accommodated in the MOR binding pocket. We characterized the free energy landscape of fentanyl conformations with metadynamics simulations, as well as performed long-timescale molecular dynamics simulations to compare and evaluate several possible fentanyl binding conditions. Our results indicate that the most preferred binding pose in the MOR binding pocket corresponds well with the minima on the energy landscape of fentanyl in the absence of the receptor, while the energy landscape can be reconfigured by modifying the fentanyl scaffold. The interactions with the receptor may stabilize a slightly unfavored fentanyl conformation in an alternative binding pose. By extending similar investigations to fentanyl analogs, our findings establish a structure-activity relationship of fentanyl binding at the MOR. In addition to providing a structural basis to understand the potential toxicity of the emerging NSOs, such insights will contribute to developing new, safer analgesics.

Keywords

Fentanyl, μ -opioid receptor, molecular dynamics simulations, metadynamics, structure-activity relationship

Introduction

Selective agonists of the μ -opioid receptor (MOR), such as morphine, codeine, and meperidine, have a long history of being used as analgesics to relieve pains (Pasternak and Pan, 2013). Based on meperidine, which shares the piperidine core with morphine, Janssen and his colleagues discovered fentanyl in 1960 (Stanley, 2014). Fentanyl is easy to synthesize, and much more potent in analgesic effect, but has higher addiction liability than morphine (Baumann et al., 2018; Pasternak and Pan, 2013; Stanley, 2014). Fentanyl and its analogs dominate the current recreational drug market (The Drug Enforcement Administration's (DEA) Special Testing and Research Laboratory's Emerging Trends Program) and are the main culprits for the ongoing and growing opioid crisis (Comer and Cahill, 2019), which has been exacerbated by the COVID-19 pandemic (Haley and Saitz, 2020).

MOR, a class A G-protein coupled receptor (GPCR), couples with both G-protein and β -arrestin to regulate downstream signaling pathways. The action mechanisms of analgesics at the MOR have been extensively studied for decades (reviewed in (Pasternak and Pan, 2013)). However, whether and how the functional selectivity is involved in inducing the side effects of fentanyl and analgesics in general, such as respiratory suppression, is still being actively studied and debated (Ehrlich et al., 2019; Gillis et al., 2020; Schmid et al., 2017; Stahl and Bohn, 2021). Early computational studies, based on homology modeling, shed light on the potential binding pose of fentanyl at the MOR (Dosen-Micovic et al., 2006; Subramanian et al., 2000). In recent years, high-resolution structures of the MOR have been acquired by both x-ray crystallography (Huang et al., 2015; Manglik et al., 2012) and cryo-electron microscopy (cryo-EM) (Koehl et al., 2018), for an inactive conformation of the receptor bound with a morphinan antagonist, β -FNA (Manglik et al., 2012), and active conformations bound with agonists BU72 and DAMGO (Huang et al., 2015; Koehl et al., 2018). These structures have been leveraged to investigate the binding mechanisms, and related MOR conformations, of the opioids having therapeutic

implications, such as methadone, morphine, and TRV130 (Kapoor et al., 2020; Mafi et al., 2020).

By taking advantage of these structures, several groups have computationally investigated the binding mechanism of fentanyl, and its analogs, at the MOR, but they have not reached a consensus (de Waal et al., 2020; Ellis et al., 2018; Lipinski et al., 2019; Podlewska et al., 2020; Ricarte et al., 2021; Vo et al., 2021). While these studies commonly found that the positively charged nitrogen on the piperidine ring forms a salt bridge with Asp^{3.32} (superscripts denote Ballesteros-Weinstein numbering (Ballesteros and Weinstein, 1995)) in the binding site of the MOR, they proposed different binding modes of fentanyl and its analogs. Specifically, based on the crystal structure of the MOR in an active conformation, Vo et al. carried out extensive molecular dynamics (MD) simulations recently and proposed that, in addition to forming a salt-bridge with Asp147^{3.32} in the orthosteric binding site (OBS), fentanyl can move deeper toward the intracellular side with its positively charged nitrogen forming a hydrogen bond to His297^{6.52} (Vo et al., 2021). They found that the amide and aniline groups of fentanyl point towards the extracellular portions of transmembrane segments (TMs) 2 and 7, an orientation of which is similar to that proposed by Lipinski et al. (Lipinski et al., 2019; Vo et al., 2021) (defined as the phenyl-piperidine-amide (FPA) orientation in **Fig. 1C**). However, using long unbiased MD simulations, Ricarte and colleagues identified an opposite orientation of fentanyl in the binding site of the MOR, with the amide and aniline groups located near the middle portions of TMs 3 and 6 (Ricarte et al., 2021) (the amide-piperidine-phenyl (APF) orientation in **Fig. 1B**). The Ricarte pose is similar to that previously proposed by de Waal et al., but in a deeper position in the binding pocket (de Waal et al., 2020; Ricarte et al., 2021). In addition, the conformations of the bound fentanyl are also different in these studies. The dihedral angle between amide carbonyl and aniline was in the *trans* configuration in the Ricarte, de Waal, and Lipinski poses (de Waal et al., 2020; Lipinski et al., 2019; Ricarte et al., 2021), and *cis* in the Vo and Podleska

poses (Podlewska et al., 2020; Vo et al., 2021) (see the *trans* and *cis* definitions in **Fig. 1D**). Together, these studies proposed varied binding poses of fentanyl at the MOR, not only in opposite orientations and different positions in the binding site, but also the divergent fentanyl conformations. Thus, the binding mechanisms of fentanyl at the MOR remains an unsolved and challenging question.

The 3- and 4-positions on the piperidine ring of the fentanyl scaffold have been exploited to develop more potent fentanyl analogs, including carfentanil, 3-methylfentanyl, and lofentanil (Stanley, 2014; Van Bever et al., 1974). In particular, carfentanil has evolved from being used as an animal anesthetic to a deadly abused drug (Zawilska et al., 2021), and even has the potential of being used as a chemical weapon (Wax et al., 2003). Intriguingly, with the same addition of a 3-methyl moiety, 3-methylfentanyl has much higher potency (as high as ~200-fold, (3R,4S)-isomer) than fentanyl (Jin et al., 1981; Xu et al., 1991), while lofentanil (i.e., 3-methylcarfentanil) only has slightly better affinity at the MOR than carfentanil (Maguire et al., 1992; Yeadon and Kitchen, 1988).

Interestingly, two stereoisomers of lofentanil (**Fig. S1**), (3S,4R)-lofentanil (Ellis et al., 2018; Maguire et al., 1992) and (3R,4S)-lofentanil (Lalinde et al., 1990; Xu et al., 1991), have been investigated and reported in the literature. Notably, the lofentanil structures are also divergent in wikipedia (<https://en.wikipedia.org/wiki/Lofentanil>, (3S,4R)-isomer) and pubchem (<https://pubchem.ncbi.nlm.nih.gov/compound/Lofentanil>, (3R,4S)-isomer) as well. Curiously, there has been no previous study that compare these two stereoisomers of lofentanil side-by-side. While it is not clear whether any specific attention was given to the isomeric issue of lofentanil in previous studies, (3S,4R)-3-methylfentanyl has drastically lower affinity (> 1000 fold) than its (3R,4S)-isomer at the MOR (Xu et al., 1991). In addition, a close analog, ohmefentanyl (**Fig. S1**), were found to have a similar pharmacological profile, with its (3S,4R)-isomers having lower affinity (> 200-fold) than its (3R,4S)-isomers (Xu et al., 1999). In the

context of the potential binding poses in the MOR (see below), these different configurations would position the 3-methyl on the piperidine ring of the fentanyl scaffold to different sides of the 4-carbomethoxy group.

In this study, we first carried out systematic characterizations of the possible conformations of fentanyl and a few selected analogs with modifications at the 3- and 4-positions on the piperidine ring. In the context of the revealed energy landscapes of these ligand conformations in the absence of the receptor, based on the cryo-EM structure of the MOR in complex with the Gi protein (Koehl et al., 2018), we performed long-timescale MD simulations to identify the most favored binding poses of fentanyl and its analogs at the MOR, by comparing the stability and energetics of their possible binding orientations and conformations. We found potential impacts of modifying the fentanyl scaffold on both conformational rigidity and binding potency. We further compared MOR conformations, stabilized by either fentanyl or by DAMGO, to reveal the initial clues about the structural basis of their divergent signaling preferences.

Methods

Metadynamics simulations to characterize the free energy landscape

Fentanyl and its analogs were prepared using Ligprep of Schrodinger (version 2020-3). The protonation state of each ligand was determined by Epik of Schrodinger (version 2020-3) in pH 7.0 ± 2.0 condition, which protonates the nitrogen in the piperidine ring of the fentanyl scaffold in to the positively charged state. For fentanyl and each of its analogs, we immersed the compound in a water box with a dimension of $30 \times 30 \times 30 \text{ \AA}^3$, which also included 0.15 M of NaCl. The total number of atoms of each system is $\sim 2,300$.

Two dihedral angles of the fentanyl scaffold were selected as collective variables (CV) (**Figure 2E**). The dihedral angle between amide carbonyl and aniline was defined as CV1, and that between aniline and piperidine as CV2. In the metadynamics simulations, the height of the biased Gaussian potential was 0.01 kcal/mol, and the window width was 5 degrees for the CVs. Metadynamics simulations were performed with Desmond (Bowers et al., 2006) (version 2020-3 with the OPLS3e force field (Roos et al., 2019) and version 2021-2 with the OPLS4 force field (Lu et al., 2021), Schrodinger LLC, New York, NY, USA). For each ligand, 10 replicate runs were performed – 5 runs were started from each of the CV1 *trans* and *cis* conformations. The length of each run for the fentanyl and carfentanil systems was 100 ns. In order to reach convergence, the runs for the (3S,4R)-lofentanil and (3R,4S)-lofentanil systems were prolonged to 400 ns each. The free energy surface (FES), defined by CV1 and CV2, was rebuilt with the Metadynamics Analysis utility of Schrodinger, with in-house modifications to flexibly increase the number of bins. To integrate the results for each system, we carried out ten bootstrap samplings of the FES of the individual runs, and sampled 100 times in each bootstrap. The average of ten samplings are shown in **Figs. 2 and S2**, while the standard deviations are shown in **Fig. S3**. The FES was normalized by defining the lowest energy point on the FES as 0.

We implemented Dijkstra's algorithms (Dijkstra, 1959) to identify the minimum free energy path (MFEP) between each pair of local minima. Briefly, we choose one of the local minima as the starting vertex and identify the neighboring vertex that has the lowest energy as the next step on the path and repeat this process. To lead the path towards the targeted minimum, the path is not allowed to revisit the same vertex. The process can generate multiple paths, when more than one neighboring vertex have the same lowest energy. Energy barrier is defined as the difference between the starting vertex and the vertex with the highest energy on the path. The MFEP is identified by finding the path with the lowest energy barrier between two minima. While the MFEP between two minima is unique, the value of energy barrier depends on the starting vertex (**Figs. 2 and S2, Table S2**).

Molecular modeling of the human MOR in an active conformation

The cryo-EM structure of the mouse MOR (mMOR) in complex with the Gi protein (PDB 6DDF) was used as the main template to build our human MOR (hMOR)-Gi models. In the structure 6DDF, some MOR residues are missing in the N terminus and at H8. We added 8 missing N terminal residues (residues 59-66 in hMOR numbering), present in another MOR structure in an active conformation (PDB 5CM1), and the missing H8 residues (residues 348-354 in hMOR numbering), from the MOR structure (PDB 4DKL), to the main template using homology modelling with Modeller (version 9.24) (John and Sali, 2003). In this modeling process, the structure 5CM1 also provided some missing sidechains in the structure 6DDF, which has relatively low resolution. The added N-terminal residues are necessary to prevent the entry of lipid molecule to the binding pocket in the following molecular dynamics (MD) simulations. In addition, the divergent residues between the mMOR and hMOR in the main template are converted to the aligned human residues (V68^{1.30I}, V189^{4.45I}, I308^{EL3V}). No change or addition

was made on the Gi protein template. The hMOR model with the lowest DOPE score was selected for following studies.

Establish the defined binding modes with molecular docking and manual adjustments

The selected hMOR model was further processed through the Protein Preparation Wizard in Maestro of Schrodinger. Hydrogen bond assignment was optimized with PROPKA (Olsson et al., 2011) at pH 7.0. Energy minimization of the structure was conducted with the default constraint of 0.3 Å heavy atoms root-mean-square deviation (RMSD). Using the induced-fit docking protocol implemented in Schrodinger (Sherman et al., 2006), we first docked fentanyl in the binding site of the prepared hMOR model. The center of docking box was determined by the center of mass of the ligand bound in the structure 6DDF, DAMGO. We applied a restraint to filter the poses that have the protonated N atom on the piperidine ring forming an ionic interaction with Asp^{3.32}. We found both APF and FPA poses in the docking results, and selected or manually adjusted the CV1 dihedral angle, so to acquire both the *trans* and *cis* conformations of each pose. Based on these hMOR models bound with fentanyl in different poses and conformations, we manually modified the fentanyl scaffold to add the extra moieties with the 3D builder in Maestro of Schrodinger (version 2020-3), and established the corresponding hMOR models bound with carfentanil, (3S,4R)-lofentanil, or (3R,4S)-lofentanil.

Molecular dynamics simulation protocol

The hMOR models with the defined binding poses of fentanyl and its analogs were further processed to build the simulation systems with the Desmond System Builder of Schrodinger suites (version 2020-3 with OPLS3e force field and version 2021-2 with OPLS4 force field). Briefly, the MOR-Gi complex models were immersed in explicit 1-palmitoyl-2-oleoyl-sn-glycero-

3-phosphocholine lipid bilayer (POPC). The simple point charge (SPC) water model was used to solvate the system, the net charge of the system was neutralized by Cl⁻ ions, and then 0.15 M NaCl was added. Residues Asp116^{2.50} and Asp166^{3.49} are protonated to their neutral forms as assumed in the active state of rhodopsin-like GPCRs (Dror et al., 2011), and we manually adjusted the His299^{6.52} protonation form to either HIE or HID as well (see Results). We additionally protonated Asp342^{7.57}, which is positioned in between TM7 and H8 and was predicted to be in a neutral protonated state in all MOR structures (6DDF, 5C1M, and 4DKL) by PROPKA. Our test run with Asp342^{7.57} deprotonated shows that the negative charge at this location likely destabilized the local interaction network with Gi. The process resulted in a system with a dimension of 106x117x151 Å³ and total number of atoms of ~190,000. The initial parameters for carfentanil and lofentanil were further optimized by the force field builder of the Schrodinger Suites (version 2020-3 with OPLS3e force field and version 2021-2 with OPLS4 force field).

Desmond MD systems (D. E. Shaw Research, New York, NY) was used for the MD simulations. Similar to our previous simulation protocols used for GPCRs (Lane et al., 2020), the system was initially minimized and equilibrated with restraints on the ligand heavy atoms and protein backbone atoms. The NP γ T ensemble was used with constant temperature maintained with Langevin dynamics. Specifically, 1 atm constant pressure was achieved with the hybrid Nose-Hoover Langevin piston method on an anisotropic flexible periodic cell with a constant surface tension (x-y plane). In the production runs at 310 K, all restraints on the hMOR were released; however, to retain the integrity of the Gi protein, while allowing adequate flexibility to interact with the receptor, the heavy atoms of residues 46-55, 182-189, and 230-242 of G α , and the entire G β and G γ subunits, were restrained with a force constant of 1 kcal/mol/Å.

For each condition, we collected at least three trajectories starting from different random number seeds. Overall, more than 200 trajectories, with an aggregated simulated time of more than 300 μ s, were collected (**Table S3**).

Conformational analysis

Dihedral angles and distances were calculated with VMD-python (version 3.0.6) (Humphrey et al., 1996). We used the Protein Interaction Analyzer (Michino et al., 2017; Stolzenberg et al., 2016) in analyzing the MD simulation results of the MOR. For analysis of coarse-grained interaction network of the hMOR, we defined the following structural elements: TM1e (the extracellular section (e) of TM1, residues 68-74), TM1m (the middle section (m) of TM1, residues 75-84), TM1i (the intracellular section (i) of TM1, residues 85-97), TM2i (residues 105-117), TM2m (residues 118-126), TM2e (residues 127-131), TM3e (residues 140-148), TM3m (residues 149-157), TM3i (residues 158-172), TM4i (residues 183-193), TM4m (residues 194-200), TM4e (residues 201-207), TM5e (residues 229-240), TM5m (residues 241-248), TM5i (residues 249-259), TM6i (residues 275-293), TM6m (residues 294-301), TM6e (residues 302-307), TM7e (residues 314-323), TM7m (residues 324-331), and TM7i (residues 332-341).

We assembled the representative ensembles of frames for analysis by randomly selecting 5,000 frames with replacement (bootstrapping) for each condition from all the trajectories of that condition, which was repeated 10 times. The same datasets were used for all the geometric calculations and analyses. The presented results are the average of the 10 bootstrap samplings.

Pairwise Root Mean Square Deviations (RMSDs) can avoid the bias of a single reference. To evaluate the stability of ligand binding, we aligned all possible pairs of the representative MD frames for a given condition according to the C α atoms of the binding site residues of hMOR: Thr122^{2.56}, Phe125^{2.59}, Gln126^{2.60}, Asn129^{2.63}, Trp135^{EL1.50}, Val145^{3.28}, Ile146^{3.29}, Asp149^{3.32},

Tyr150^{3.33}, Met153^{3.36}, Asp218^{EL2.49}, Cys219^{EL2.50}, Trp295^{6.48}, Ile298^{6.51}, His299^{6.52}, Trp320^{7.35}, His321^{7.36}, Ile324^{7.39}, Gly327^{7.42}, and Tyr328^{7.43}, then calculated the RMSD based on the ligand heavy atoms.

MM/GBSA calculation

Binding free energies between the bound ligands and the hMOR were estimated with the Molecular mechanics/generalized Born surface area calculations (MM/GBSA) method, using the same force field in the MD simulations for the proteins and ligands, but with VSGB2.1 solvation model (Li et al., 2011). We extracted frames every 3 ns from the production runs to carry out the MM/GBSA calculations using the thermal_mmgsa.py script from the Schrodinger suite. The binding free energies for each condition were the averages of the selected frames.

Results

The amide moiety of fentanyl and its analogs favors the *trans* conformation

Previous MD simulation studies showed that the amide moiety of fentanyl could be stable in either the *trans* or *cis* conformation (**Fig. 1D**) in the MOR binding pocket, without any reported transition between these two conformations (de Waal et al., 2020; Lipinski et al., 2019; Podlewska et al., 2020; Ricarte et al., 2021; Vo et al., 2021). These results suggest the transition between the *trans* and *cis* conformations may have a relatively high energy barrier to overcome in the MD simulations, but these studies did not evaluate which conformation has lower energy. Interestingly, in a crystal structure of a computationally designed fentanyl binding protein, the amide moiety of the bound fentanyl is in *trans* (Bick et al., 2017).

Metadynamics simulation is an enhanced sampling method that can efficiently overcome energy barriers by adding time-dependent bias potential acting on selected collective variables (CVs) (Laio and Parrinello, 2002). Thus, to thoroughly understand the energy landscape of the fentanyl conformation, we carried out metadynamics simulations with a fentanyl molecule immersed in a water box (see Methods). In these simulations, we defined two CVs, CV1 is the dihedral angle between the amide carbonyl and aniline moieties (**Fig. 2E**), while CV2 is the dihedral angle between aniline and piperidine (**Fig. 2F**).

As expected, in our metadynamics simulation results plotted on a 2D free energy surface (FES) (**Fig. 2**), we observed that CV1 has two energy minima, near 0° (*cis*, referred to as the “C” state below) and 180° (*trans*, the “T” state). Interestingly, CV2 has two minima as well, near -50° (denoted as the “L” state) and 105° (the “H” state). The examination of the FES indicates that the T state has lower energy than the C state, while the L state has lower energy than the H state and has a very wide range (~ 0 - 120°) (**Fig. 2A** and **Table S1**). Thus, on the FES determined by CV1 and CV2, the T state of CV1, in combination with L state of CV2 (referred to as TL), has the globally lowest energy (**Fig. 2A** and **Table S1**).

Using the Dijkstra's algorithm, we identified the minimum free energy paths (MFEP) (Branduardi and Faraldo-Gómez, 2013) between the energy minima and calculated the height of the energy barrier along each of such paths on the FES (see Methods). The results show that the transition between the TL and TH states has a significantly lower energy barrier than other transitions, while the C to T transitions (both of the CH to TH and CL to TL MFEPs) have > 11 kcal/mol energy barrier (**Fig. 2A** and **Table S2**).

To understand the impact of the modifications of the fentanyl scaffold on the FES, we carried out similar metadynamics simulations of two fentanyl analogs, carfentanil and lofentanil. Carfentanil has a carbomethoxy group at the 4-position of the piperidine ring; in addition to this modification, lofentanil has an extra methyl group at the 3-position of the piperidine ring, the chirality of which results in the (3S,4R)- and (3R,4S)-isomers of the compound (**Fig. S1**). Compared to the FES of fentanyl, those of carfentanil and lofentanil have similar CV1 profiles, i.e., the T and C states are similarly located, while the T states always have lower energy than the C states (**Fig. 2B-D**, **Table S1**). However, both carfentanil and lofentanil have drastically different CV2 profiles from that of fentanyl, suggesting significant impacts of the modifications on both the conformation and the flexibility of the scaffold. Specifically, the regions of the H states on the FES of fentanyl are high-energy forbidden regions for both carfentanil and lofentanil. Further, an energy barrier arises in the middle of the L state and splits the state into two, which we termed L1 and L2 states. The L1 and L2 states of carfentanil and lofentanil are similarly located near $-5-10^\circ$ and $-110-120^\circ$, respectively. Given the same CV1 state (either the T or C state), the L1 and L2 states of carfentanil have comparable energies, but L1 has ~ 6 kcal/mol higher energy than L2 for (3S,4R)-lofentanil, while (3R,4S)-lofentanil has a reversed trend between the L1 and L2 states compared to those of (3S,4R)-lofentanil, demonstrating the impact of the methyl modification on the scaffold. In addition, their energetic differences

between the most favored T states (TL2 for carfentanil and (3S,4R)-lofentanil, TL1 for (3R,4S)-lofentanil) and the C states are larger than that of fentanyl (**Table S1**).

On the FES of carfentanil, the identifications of MFEPs and calculations of energy barrier show that the transition from the CL1 to the TL1 state, which is favored in the MOR binding site (see below), has more than 2 kcal/mol lower energy barrier than the CL to TL transition of fentanyl (**Table S2**), suggesting the carbomethoxy modification may facilitate this transition. The additional methyl group on the piperidine ring of (3S,4R)-lofentanil further lowered the energy barrier of the CL1 to TL1 state transition to ~7 kcal/mol, while that for (3R,4S)-lofentanil is similar to carfentanil (**Table S2**).

To further dissect the roles of 3-methyl and 4-carbomethoxy in altering the FES, we performed metadynamics simulations of (3S,4R)- and (3R,4S)-isomers of 3-methylfentanyl. The examination of their FESs show that 3-methylfentanyl isomers have similar FESs to that of fentanyl. However, the positions of their L and H states of CV2 are altered, while the CL states of 3-methylfentanyl have slightly narrow distributions than that of fentanyl (**Fig. 2**). Interestingly, the minima of the L states (both TL and CL) on the FES of (3R,4S)-3-methylfentanyl are pushed to similar minima positions of the L1 states of carfentanil and lofentanil, while those of (3S,4R)-3-methylfentanyl are pushed to those of the L2 states (**Fig. 2** and **Table S1**). These different impacts are consistent with L1 and L2 states having lower energies for (3R,4S)- and (3S,4R)-lofentanil, respectively.

Taken together, the T state is the most favored state for fentanyl and all its studied analogs, while the modifications on the piperidine ring in carfentanil and lofentanil make this trend even stronger and lowered the energy barrier for the transition from the C to T state. While this manuscript was being prepared, an updated OPLS force field (OPLS4) became available (Lu et al., 2021). Using OPLS4, we carried out the same set of metadynamics simulations and

analyses and found similar results and conclusions as those described above using OPLS3e (**Fig. S2, Tables S1 and S2**).

Fentanyl can be stable in two opposite binding orientations in the MOR binding pocket

To comprehensively evaluate the possible binding poses of fentanyl in the active conformation of the MOR, we first docked fentanyl in the cryo-EM structure of the MOR-Gi complex (PDB 6DDF) (Koehl et al., 2018) (see Methods). By selecting and then manually adjusting the docked poses, we established fentanyl poses in both the APF and FPA orientations (see the definitions in **Fig. 1B,C**) and in both *trans* and *cis* conformations, as proposed by previous studies (de Waal et al., 2020; Lipinski et al., 2019; Podlewska et al., 2020; Ricarte et al., 2021; Vo et al., 2021) (see the definition in **Fig. 1D**). In addition, Vo et al. showed that the protonation state of the His^{6.52} might have a significant impact on the fentanyl binding pose (Vo et al., 2021), which prompted us to consider two neutral protonation states (HIE and HID) of His^{6.52} in our study as well. Thus, we built the fentanyl bound MOR-Gi complex models in 8 conditions (**Table S3**) and immersed the resulting models in the explicit lipid bilayer simulation environment (see Methods). For each condition, we collected multiple prolonged MD simulation trajectories, using either or both OPLS3e and OPLS4 force fields (**Table S3**). For the condition that we have both OPLS3e and OPLS4 data, we did not find any noticeable difference resulting from different force fields. We analyzed the data separately but drew the conclusions by integrating all the results. To evaluate the stability of binding modes, we calculated the pairwise ligand RMSDs of all possible pairs of MD frames of the representative ensembles for each condition (see Methods). Our results show that fentanyl in the APF *trans* conditions (both APF_{ET} and APF_{DT}, “E” and “D” in the subscripts represent the His^{6.52} in its HIE and HID forms, respectively) are very stable with the pairwise ligand RMSDs of 1.0 and 0.9 Å, respectively (**Figure 3A**), while this measure is noticeably larger for the APF *cis* modes (2.6 and 1.5 Å for APF_{EC} and APF_{DC}, respectively).

Interestingly, the bound fentanyl in the APF_{EC} condition has a strong tendency to transition to the *trans* conformation (**Fig. S4**), therefore this condition is not considered to be stable for further analysis. We then carried out MM/GBSA binding energy calculations for the same set of representative MD frame ensembles of each condition. The results show that the APF_{DT} condition has the most favored binding energy, and the APF_{ET} and APF_{DC} conditions have 2.5 and 8.1 kcal/mol higher energies ($\Delta\Delta G$), respectively. Thus, both the pairwise ligand RMSD and MM/GBSA results are consistent with the findings from our metadynamics simulations (**Fig. 2B** and **Table S1**) in which we found that the T state has lower energy. When comparing the APF_{ET} and APF_{DT} conditions, we found the bottom of the binding pocket near His299^{6.52} is less dynamic in APF_{DT} than in APF_{ET}. In particular, the distribution of His299^{6.52} χ 1 rotamer in APF_{DT} is tighter than in APF_{ET}, which also results in a slightly different orientation of Trp295^{6.48} χ 2 (**Fig. S5**).

In contrast to the APF conditions, among the FPA conditions of fentanyl, only FPA_{DC} appears to be a reasonably stable condition with a pairwise ligand RMSD of 1.8 Å, while the other three FPA conditions have drastically higher RMSDs (**Figure 3B**). This trend is reflected on the MM/GBSA calculation results in which the FPA_{ET}, FPA_{DT}, and FPA_{EC} modes have more than 6 kcal/mol higher energies than the FPA_{DC} mode. However, the possibility that the fentanyl can be stable in FPA_{DC} is surprising given our findings from the conformational search and metadynamics simulations, which show the *cis* conformation of fentanyl has higher energy (**Fig. 2A**). From our inspection of the FPA_{DC} condition, we found that the *cis* conformation of the amide group of fentanyl forms a hydrogen bond (H-bond) interaction with the sidechain of either Gln126^{2.60} or Asn129^{2.63} (**Figs. 3D** and **S4**), which appears to compensate the less favored fentanyl *cis* conformation. Similar to what we observed between the APF_{ET} and APF_{DT} conditions, the bottom of the binding pocket in FPA_{EC} is more dynamic than in FPA_{DC}, with the His299^{6.52} χ 1 in wider distribution (**Fig. S5**). This perturbation by the HIE form of His299^{6.52} is

propagated to the extracellular side of the binding pocket and disrupts the interactions between the amide carbonyl of fentanyl and Gln126^{2.60}/Asn129^{2.63} (**Fig. S5**).

In summary, we found that fentanyl can be stable in both APF and FPA orientations, with the APF_{DT} and FPA_{DC} conditions being more favored than the other conditions in each orientation. While the bound fentanyl in both APF_{DT} and FPA_{DC} conditions form the ionic interaction with Asp149^{3.32}, and several other residues in the OBS (Michino et al., 2015), our detailed contact frequency analysis (see Method) indicate that several residues form distinct interactions either in the APF or FPA poses (**Table 1**).

We then collected previously reported mutagenesis work relevant to fentanyl binding at the MOR by extracting the curated information from GPCRdb (Pándy-Szekeres et al., 2017), as well as carrying out our own literature search (**Table S4**). Indeed, by comparing the frequently contacting residues in APF and FPA poses, we found mutations of the residues that are not directly involved in interacting with either pose, Ile^{4.56}, Val^{4.60}, and Lys^{6.58} have no effect on fentanyl binding (Bonner et al., 2000; Mansour et al., 1997). However, the substitutions of His^{6.52} to Asn or Gln have no effect as well, indicating a polar residue can be tolerated at this position, while the aromatic property of His is not critical (Spivak et al., 1997). Interestingly, Ala mutation of residue His^{7.36}, which interacts with the bound fentanyl in the FPA_{DC} condition but has no chance of interacting in APF_{DT} in our simulations, resulted in significant disruption of the ohmefentanyl binding at the MOR (Xu et al., 1999) (**Table S4**). From our modeling the ohmefentanyl pose in the MOR binding site, in either the APF or FPA pose, the potential interaction with His^{7.36} could not be from the extra modifications of ohmefentanyl on the fentanyl scaffold, i.e., the 3-methyl of the piperidine ring and 2-hydroxy on the linker between phenyl and piperidine. Thus, the FPA pose may explain the His^{7.36}Ala mutagenesis data better, however, we cannot exclude the possibility of indirect effect of the mutation.

The APF *trans* binding poses of carfentanil and lofentanil are more stable

To characterize the impact of modifications on the fentanyl scaffold on the binding pose preferences at the MOR, we then carried out MD simulations of the MOR in complex with carfentanil or lofentanil, each in all 8 conditions as those for the MOR-fentanyl complex (**Table S3**).

In the APF *cis* conditions (both APF_{EC} and APF_{DC}), both carfentanil and (3S,4R)-lofentanil could not stay in the *cis* conformation and transitioned to the *trans* conformation in all the trajectories within 3 μ s, while the transitions in the APF_{EC} condition were noticeably faster than in APF_{DC} (**Fig. S4**). This is consistent with the results of our metadynamics simulations that show the differences between *cis* and *trans* conformations are higher for carfentanil and lofentanil than for fentanyl (**Table S1**), while the transitions from the C to T state are easier, i.e., having lower energy barriers than those of fentanyl (**Table S2**).

In the FPA *cis* conditions, FPA_{EC} is not stable for carfentanil and both isomers of lofentanil, and the bound compounds in the majority of the FPA_{EC} trajectories transitioned to *trans* conformation. In the FPA_{DC} condition, however, while (3S,4R)-lofentanil transitioned to *trans* conformation in all trajectories and (3R,4S)-lofentanil has high pairwise ligand RMSDs (**Fig. 4**), carfentanil can be stable in the FPA_{DC} condition in all trajectories as fentanyl, to the extent of our simulations (**Figure S4**). Indeed, we noticed that carfentanil could form a similar H-bond interaction with either Gln126^{2.60} or ASN129^{2.63}, as fentanyl in FPA_{DC}. An analysis of the dihedral angle between aniline and piperidine (i.e., the CV2 in the metadynamics simulations) of the FPA_{DC} conditions of both fentanyl and carfentanil revealed that these bound ligands form the H-bond with either Gln126^{2.60} or ASN129^{2.63} only in the CL1 state (**Figs. S6 and S7**), which can be significantly populated in the metadynamics simulations (**Fig. 2**). In contrast, the CL1 state of (3S,4R)-lofentanil has at least more than 6.5 kcal/mol higher energy than the other energy

minima on the FES, and is a highly unstable state (**Fig. 2**, and **Table S1**). The potential H-bonds that can be formed to Gln126^{2.60} or ASN129^{2.63} could not retain (3S,4R)-lofentanil in this state. Comparing the APF and FPA *trans* conditions, similar to the situation of fentanyl, two FPA conditions (FPA_{ET} and FPA_{DT}) of carfentanil and both lofentanil isomers have significantly higher pairwise ligand RMSDs than two APF conditions, indicating the former are likely not stable poses (**Figure 4**). Interestingly, in the MM/GBSA calculations, however, we found the APF_{ET} condition is slightly more favored than APF_{DT} for carfentanil, and lofentanil (APF_{ET} has 1.9, 2.6, and 1.7 kcal/mol lower energy than APF_{DT} for carfentanil, (3S,4R)-lofentanil, and (3R,4S)-lofentanil, respectively), which is different from the situation in fentanyl.

For these two preferred APF *trans* conditions, the analysis of the dihedral angle between the aniline and piperidine shows that carfentanil and both isomers of lofentanil stay in their TL1 states and never get into the TL2 state, while fentanyl is in a much wider distribution (**Figs. S6 and S7**). From the FES of these compounds, we note that the TL1 state is the most preferred state for (3R,4S)-lofentanil, while the TL1 state has only slightly higher energy than the TL2 state for carfentanil. However, the TL1 state of (3S,4R)-lofentanil has 6.9 kcal/mol higher than its TL2 state and is likely stabilized or restricted by the interactions with the MOR binding residues (**Fig. 2** and **Table S1**).

Thus, carfentanil is like fentanyl and can be stable in both the APF and FPA orientations, but both isoforms of lofentanil can only be in the APF orientation due the conformational restraints rendered by the extra methyl group on the piperidine ring.

Carfentanil has been reported to have at least 6-fold (Baumann et al., 2018; Yeadon and Kitchen, 1988) or even ~50-fold (Maguire et al., 1992) higher binding affinity than fentanyl at the MOR, while lofentanil was at least equally more potent (Maguire et al., 1992) or has an even slightly higher affinity than carfentanil (Yeadon and Kitchen, 1988). By comparing the contact frequencies in the APF_{DT} conditions of carfentanil and lofentanil versus that of fentanyl, we

found the carbomethoxy group of carfentanil and both lofentanil isomers a strong interaction with Trp^{7.35} (**Figure 4** and **Table 1**), which is likely the structural basis for their enhanced affinities at the MOR. The extra methyl group of (3R,4S)-lofentanil form a weak interaction with Tyr150^{3.33}, which may further stabilize the APF_{DT} condition compared to those of carfentanil, though only marginally (see Discussion).

MOR conformational change when binding to the fentanyl and its analogs

DAMGO, which is bound in the cryo-EM structure of the MOR-Gi complex used as the main template for this study, has been found to be an unbiased full agonist (Kelly, 2013), while fentanyl has been proposed to be an β -arrestin-biased agonist at the MOR (Schmid et al., 2017). In order to fully understand the functional consequence of fentanyl binding, it is critical to evaluate whether fentanyl binding would result in a different receptor conformation compared to that stabilized by DAMGO. Thus, we compared the conformations of the MOR-fentanyl and MOR-DAMGO models. For the former, we chose the more favored MOR-fentanyl APF_{DT} condition; for the latter, based on the original cryo-EM structure, we immersed a refined MOR-DAMGO model in a lipid bilayer and carried out extensive MD simulations using the same simulation protocols as those for the MOR-fentanyl models (**Table S3**). In these control simulations of the MOR-DAMGO model, we found only limited changes from the original conformation revealed by the cryo-EM structure, as demonstrated by the low and quickly plateaued RMSD evolutions along the MOR-DAMGO MD trajectories (**Fig. S8**).

We adapted a previously developed in-house tool, the Protein Interaction Analyzer (see Methods), to compare the representative MD frame ensembles of the MOR-fentanyl and MOR-DAMGO models, with a focus on the regions in or near the binding pocket (see Methods). We found the conformations of the OBS in two models are very similar (the region enclosed by the dotted box in **Fig. 5C**); however, there are significant changes in a secondary binding pocket

(SBP) near the extracellular portion of TM1 (TM1e, see the definition in Method section), TM2e, TM3e, and TM7e. Our inspections of the models indicated that these changes likely resulted from an outward rearrangement of Trp135^{EL1.50} due to its interaction with the phenyl moiety of fentanyl, while Tyr130^{2.64} rotates inward, compared to their configurations in the presence of the bound DAMGO (**Fig. 5**). These coordinated changes are reflected in the shortened distance between Tyr130^{2.64} and Trp135^{EL1.50} in the presence of fentanyl (**Fig. 5F**). We further quantified the differential effects of fentanyl and DAMGO bindings by plotting the distances of TM1e-TM3e versus TM2e-TM7e in two conditions. We found fentanyl reduced the TM1e-TM3e distance, elongated the TM2e-TM7e distance, and therefore changed both the size and shape of the SBP (**Fig. 5D,E**).

Discussion

The mechanistic understanding of the binding of fentanyl and its analogs at the MOR is the foundation to reveal how the impact of these abused synthetic opioids is propagated toward the intracellular side of the receptor to initiate downstream signaling cascades, which will then elicit both beneficial analgesic and a variety of undesired side effects. However, in the absence of high-resolution structural information of the MOR bound with fentanyl, previous molecular modeling and simulation studies have proposed drastically different fentanyl binding modes, both in orientations within the binding pocket and ligand conformations (de Waal et al., 2020; Lipinski et al., 2019; Podlewska et al., 2020; Ricarte et al., 2021; Vo et al., 2021). To this end, we carried out a systematic computational study to investigate the preferred conformations of fentanyl and how these conformations are being accommodated in the MOR binding pocket, by characterizing the free energy landscape of fentanyl conformations with metadynamics simulations, as well as performing long-timescale MD simulations to compare 8 possible binding conditions. Our results indicate that the APF_{DT} binding condition is preferred, while the FPA_{DC} condition is also possible, with the slightly unfavored cis conformation of fentanyl stabilized by forming a H-bond with Gln126^{2.60} or Asn129^{2.63}.

Our APF *trans* poses of fentanyl are largely consistent with the fentanyl pose reported by Ricarte et al., which was based on the modeling and the simulations with the structure 5C1M (Ricarte et al., 2021), and we found that the same set of hMOR residues interact with fentanyl (**Table 1**). Our FPA_{DC} is in a similar orientation as the pose proposed by Vo et al., whom, however, found that when His^{6.52} was in the HID form, fentanyl could move deeper and form a hydrogen bond between the protonated piperidine amine to the N ϵ atom of His^{6.52}, instead of forming a salt bridge with Asp^{3.32} (Vo et al., 2021). While in our simulations, the bound fentanyl in the FPA_{DC} condition retains the interaction with Asp^{3.32} persistently. Our results show that the

protonation state of His^{6.52}, had only limited impact on the APF pose of fentanyl and carfentanil (**Figs. 3 and 4**); however, the HID form facilitated stabilizing the FPA pose (**Fig. 3**).

Our results also provide the structural basis for why 3-methyl modification prefers the (3R,4S)- but not (3S,4R)- configuration in improving the potency of the fentanyl scaffold. All our modeled and simulated fentanyl analogs stay in the TL1 state in the APF poses (**Figs. S6 and S7**). While the TL1 state of (3R,4S)-lofentanil and the T state of (3R,4S)-3-methylfentanyl on the FESs have lower energy than the TL2 state, their (3S,4R)-isomers have the reversed trend (**Fig. 2C,D**). Thus, the (3S,4R)-isomer is not in its preferred state in the binding pocket of the MOR. In addition, the stronger interaction with Tyr^{3.33}, when the ligand is in the (3R,4S)-configuration, is expected to further improve the affinity. However, the drastic improved affinity of 3-methylfentanyl over fentanyl, which is not observed in lofentanil over carfentanil, indicate that modifications at the 3- and 4-positions may have overlapping roles in improving the potency; at least they do not have additive effects. Interestingly, in our MM/GBSA calculations, we found that the (3R,4S)- and (3S,4R)-lofentanil do not have significantly different binding energies in their APF poses, suggesting that the 4-carbomethoxyl may mask the effect of 3-methyl in different configurations. Thus, we speculate that the affinity difference between (3R,4S)- and (3S,4R)-lofentanil may not be as drastic as that between (3R,4S)- and (3S,4R)-3-methylfentanyl.

In this study, we compared the results from metadynamics and MD simulations of fentanyl in the absence and presence of the receptor, respectively, and combined them to establish the structure-activity relationship (SAR) of the fentanyl scaffold at the MOR. The FES deduced from metadynamics simulations lay the foundation for our understanding of how fentanyl and its analogs would behave in the binding pocket of the MOR. The most favored poses of fentanyl and its analogs are consistent with the global minima on the FES, the FES guided us to seek the specific ligand-receptor interactions that may compensate the unfavored ligand

conformations. Such an approach to thoroughly characterize the energy landscape of the ligand conformation has not been well appreciated. While long-timescale MD simulations is powerful in revealing ligand-induced receptor conformation changes to accommodate specific ligand scaffolds, it is not trivial to identify the proper binding pose with MD simulations in the first place, such as our previous work in identifying the binding modes of paroxetine at the serotonin transporter (Abramyan et al., 2019). Indeed, even at relatively long timescales, we have not observed any transition between APF and FPA orientations. Thus, this combined approach provides a framework not only for the current fentanyl study but can also be applied to other SAR studies at other GPCRs.

In a companion manuscript, by combining the experimental and computational approaches, we found that the alkyl modifications of the amide moiety of the fentanyl scaffold affect the efficacy at the MOR (Xie et al., manuscript in preparation). Together, our findings start to establish a SAR of fentanyl binding at the MOR, which will facilitate our prediction and understanding of the potential toxicity of emerging novel synthetic opioids based on the fentanyl scaffold. Such insights will also contribute to developing new, safer analgesics with desired pharmacological properties.

Author Contribution

B.X. and L.S. designed the study. B.X. and A.G. carried out computational modeling, simulations, and analysis. All authors took part in interpreting the results. B.X. and L.S. wrote the manuscript.

Declarations of Competing Interests

No potential conflict of interest was reported by the authors.

Acknowledgements

We thank Michael Baumann for insightful discussions. Support for this research was provided by the National Institute on Drug Abuse–Intramural Research Program, Z1A DA000606 (L.S.). This work utilized the computational resources of the NIH HPC Biowulf cluster (<http://hpc.nih.gov>).

Figures and Figure Legends

Figure 1. Two possible binding orientations of fentanyl in the orthosteric binding site of μ -opioid receptor. (A) An overview of a fentanyl bound MOR-Gi complex. The binding pocket is highlighted with a dashed box. (B) and (C) are schematic orientations of how a bound fentanyl can be oriented in the MOR binding pocket. F, P, and A stand for phenyl, piperidine, and amide moieties of fentanyl, respectively. Two binding orientations, APF (B) and FPA (C), have been proposed in previous studies (see text). In addition, the rotation of the bond between the amide carbonyl and aniline results in *trans* and *cis* conformations of fentanyl, as shown in panel D.

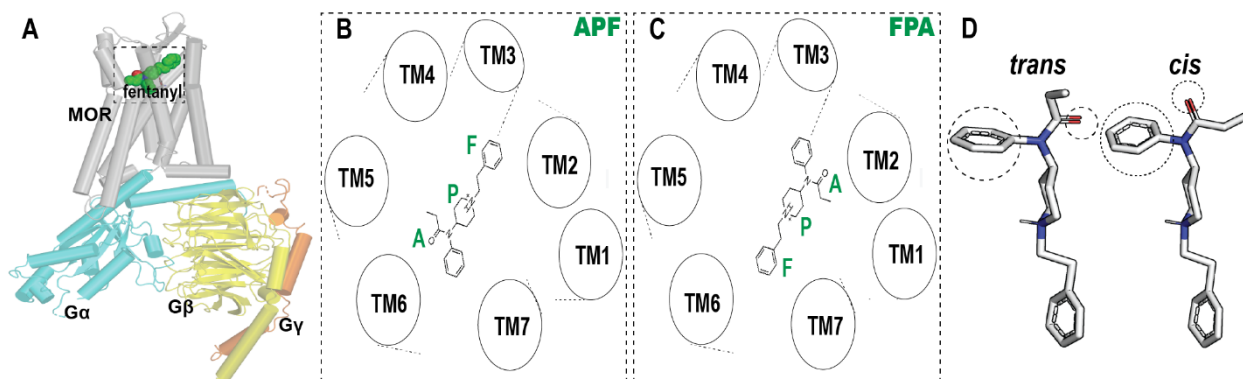


Figure 2. Metadynamics simulations of fentanyl and its analogs reveal their possible conformations. The free energy surfaces (FESs) reconstructed from the metadynamics results are shown in panels A-D for the indicated ligands. For each FES, we identified four minima, labelled as TL, TH, CL, CH for fentanyl, TL1, TL2, CL1, CL2 for the other analogs. The dihedral angle between amide carbonyl and aniline is defined as CV1, and that between aniline and piperidine as CV2, as shown in panel E. The conformations of the ligands in the MOR binding pocket are the TL state for fentanyl and TL1 for the other analogs (see text). The minimum free energy paths (MFEP) between the TL and CL states for fentanyl and the TL1 and CL1 states for the other analogs are plotted with dotted curves on each FES. The conformations corresponding to the energy minima are shown in panel E for fentanyl (3-methylfentanyl has similar four states), and panel F for carfentanil (lofentanil has similar four states).

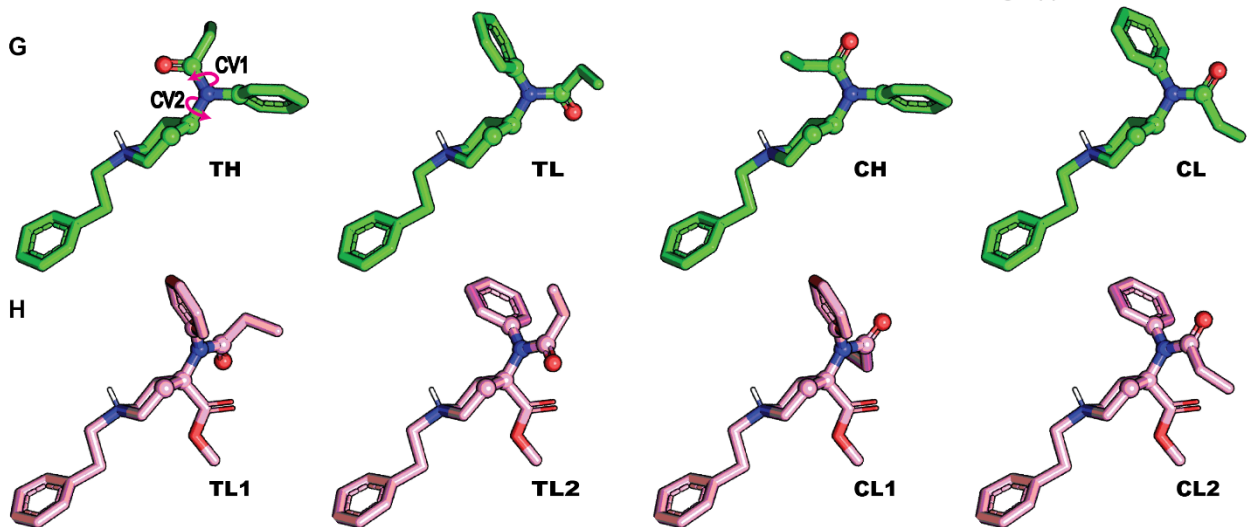
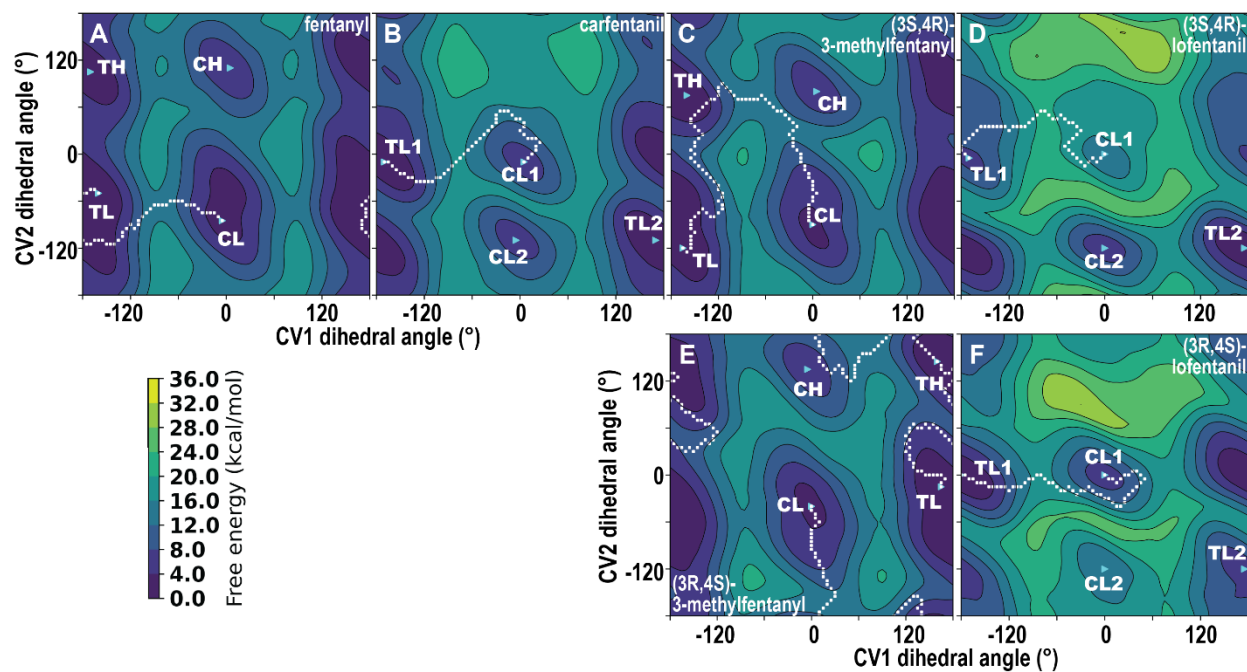


Figure 3. APF_{DT} and FPA_{DC} are the more stable poses in each orientation. The average pairwise ligand RMSDs for each indicated condition are shown for the APF and FPA orientations in panels A and B, respectively. The APF_{DT} and FPA_{DC} are the more stable conditions for APF and FPA orientations, respectively, and the fentanyl binding poses in these two conditions are demonstrated in panels C and D.

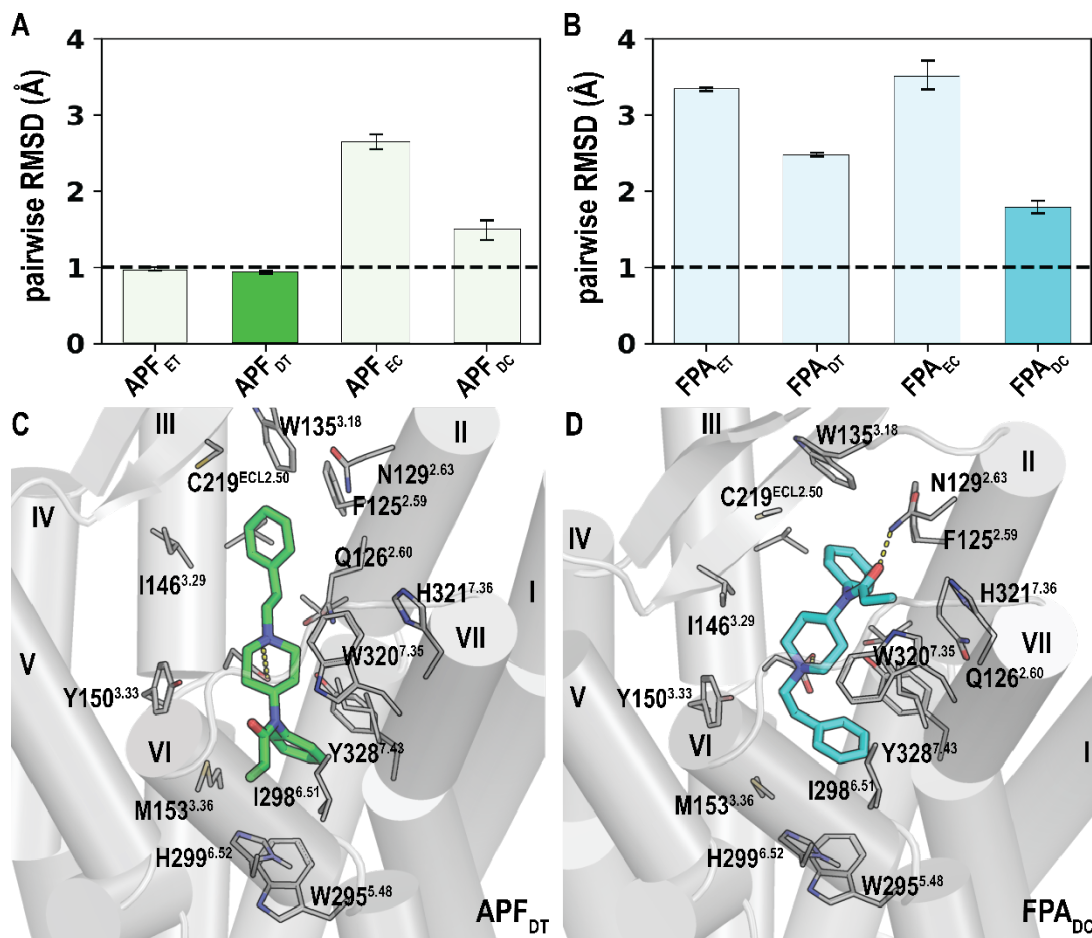


Figure 4. Carfentanil and lofentanil prefer the APF orientation. The average pairwise ligand RMSDs for each indicated ligand and condition are in panels A-C. APF_{DT} conditions for each analog are shown in panels D-F. As a reference, the fentanyl binding pose (green) is superimposed in each panel. The carbomethoxy moiety of these analogs form an additional contact to Trp320^{7.35} (large circles in panels D-F), which is likely responsible for the higher potencies of these analogs compared to fentanyl. In addition, (3R,4S)-lofentanil has a strong interaction between its 3-methyl to Tyr150^{3.33} (small circle in panel F), which likely contributes to its slightly higher affinity than carfentanil.

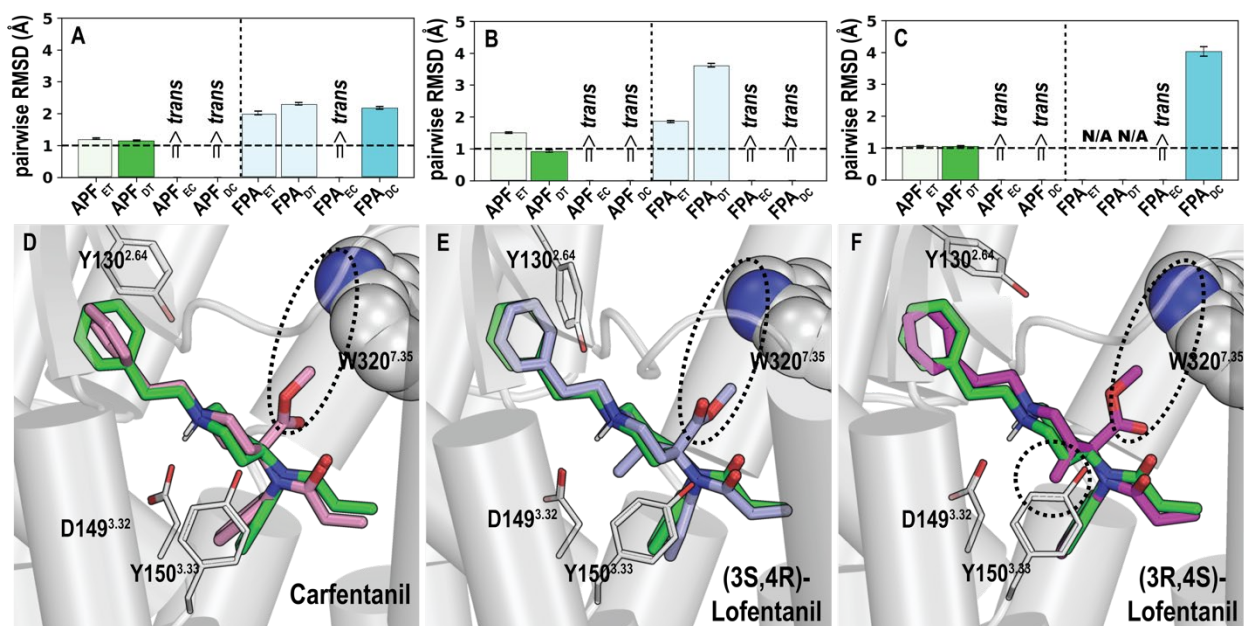
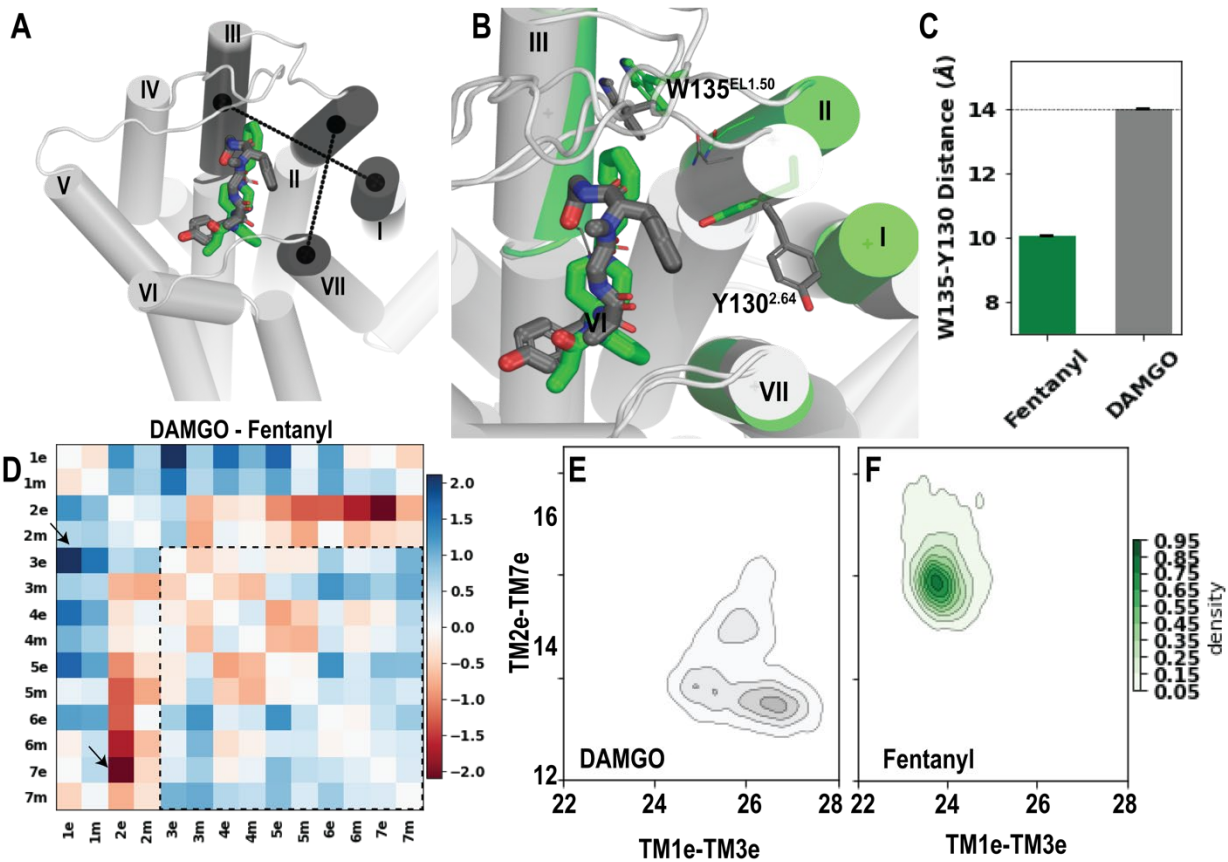


Figure 5. Fentanyl induced divergent conformation near the binding pocket. (A) An overview the superimposed DAMGO and fentanyl binding poses in the MOR. (B) A zoom-in view demonstrating the diverged positions and orientations of Tyr130^{2.64} and Trp135^{EL1.50} when the receptor is bound with either DAMGO or fentanyl (APF_{DT}). Panel C shows the center-of-mass distances between the phenyl ring of the indole moiety of Trp135^{EL1.50} and the sidechain of Tyr130^{2.64} in the fentanyl and DAMGO bound conditions. In the analysis with the Protein Interaction Analyzer, we calculated the center-of-mass distances among the extracellular and middle subsegments of the MOR. The differences of these distances between the DAMGO and fentanyl bound conditions (i.e., distance_{DAMGO} - distance_{fentanyl}) are plotted on a heatmap shown in panel D. Specifically, the differences in the orthosteric binding site enclosed by TMs 3, 5, 6, and 7 (dotted box) are small, however, significant differences are detected in a secondary binding pocket encircled by TMs 1, 2, 3, and 7. In particular, the TM1e-TM3e distance is larger in the presence of the bound DAMGO, while TM2e-TM7e is larger in the fentanyl-bound condition. These two distances are indicated by the dotted lines in panel A, and their distributions are shown in panels E and F for DAMGO- and fentanyl-bound conditions, respectively.



Tables

Table 1. The contact frequencies of the residues interacting with fentanyl and its analogs in the hMOR. In a molecular dynamics (MD) simulation frame, if the shortest heavy-atom distance between the ligand and any given residue of the MOR was within 5 Å, we defined that the ligand forms an interaction with this residue. The residues that have at least one contact frequency > 0.6 in any indicated condition are included in this table. The results shown here are based on the simulations with the OPLS4 force field. For the APF poses, we combined the results of APF_{ET} and APF_{DT} into APF_T for each indicated ligand. The differences between the analogs and fentanyl in their APF_T conditions are shown in the “- fentanyl” columns.

Residue	fentanyl		carfentanil		(3S,4R)-lofentanil		(3R,4S)-lofentanil	
	APF _T	FPA _{DC}	APF _T	- fentanyl	APF _T	- fentanyl	APF _T	- fentanyl
Thr122 ^{2.56}	0.32	0.98	0.12	-0.20	0.02	-0.30	0.16	-0.16
Phe125 ^{2.59}	0.08	0.97	0.13	0.06	0.12	0.05	0.10	0.02
Gln126 ^{2.60}	1.00	0.99	1.00	0.00	1.00	0.00	1.00	0.00
Asn129 ^{2.63}	0.96	0.89	0.98	0.02	0.96	0.00	0.99	0.03
Tyr130 ^{2.64}	0.47	0.14	0.53	0.06	0.70	0.24	0.56	0.09
Trp135 ^{EL1.50}	0.99	1.00	0.98	-0.01	0.93	-0.06	0.96	-0.04
Val145 ^{3.28}	0.97	0.99	0.98	0.01	0.93	-0.04	0.94	-0.03
Ile146 ^{3.29}	0.99	1.00	0.99	0.01	1.00	0.02	0.98	-0.01
Asp149 ^{3.32}	1.00	1.00	1.00	0.00	1.00	0.00	1.00	0.00
Tyr150 ^{3.33}	0.28	0.97	0.52	0.24	0.54	0.27	0.87	0.59
Asn152 ^{3.35}	0.74	0.00	0.46	-0.28	0.41	-0.33	0.55	-0.19
Met153 ^{3.36}	1.00	0.99	1.00	0.00	1.00	0.00	1.00	0.00
Cys219 ^{EL2.50}	1.00	1.00	1.00	-0.01	0.99	-0.01	0.98	-0.03
Val238 ^{5.42}	1.00	0.12	0.96	-0.04	0.82	-0.18	0.92	-0.08
Trp295 ^{6.48}	0.95	0.59	0.89	-0.06	0.96	0.01	0.95	0.00
Ile298 ^{6.51}	1.00	0.98	1.00	0.00	1.00	0.00	1.00	0.00
His299 ^{6.52}	1.00	0.68	1.00	0.00	1.00	0.01	1.00	0.01
Val302 ^{6.55}	0.98	0.11	0.88	-0.10	0.95	-0.03	0.89	-0.09
Trp320 ^{7.35}	0.43	0.73	1.00	0.57	1.00	0.57	1.00	0.57
His321 ^{7.36}	0.00	0.86	0.00	0.00	0.00	0.00	0.00	0.00
Ile324 ^{7.39}	1.00	1.00	1.00	0.00	1.00	-0.01	1.00	0.00
Gly327 ^{7.42}	0.99	0.84	0.99	0.00	0.99	0.00	1.00	0.02
Tyr328 ^{7.43}	1.00	1.00	1.00	0.00	1.00	0.00	1.00	0.00

References

- Abramyan, A.M., Slack, R.D., Meena, S., Davis, B.A., Newman, A.H., Singh, S.K., and Shi, L. (2019). Computation-guided analysis of paroxetine binding to hSERT reveals functionally important structural elements and dynamics. *Neuropharmacology* *161*, 107411. 10.1016/j.neuropharm.2018.10.040.
- Ballesteros, J.A., and Weinstein, H. (1995). Modeling Transmembrane Helix Contacts in GPCR. held in San Francisco, CA, pp. TH-462.
- Baumann, M.H., Kopajtic, T.A., and Madras, B.K. (2018). Pharmacological Research as a Key Component in Mitigating the Opioid Overdose Crisis. *Trends Pharmacol Sci* *39*, 995-998. 10.1016/j.tips.2018.09.006.
- Bick, M.J., Greisen, P.J., Morey, K.J., Antunes, M.S., La, D., Sankaran, B., Reymond, L., Johnsson, K., Medford, J.I., and Baker, D. (2017). Computational design of environmental sensors for the potent opioid fentanyl. *Elife* *6*. 10.7554/eLife.28909.
- Bonner, G., Meng, F., and Akil, H. (2000). Selectivity of mu-opioid receptor determined by interfacial residues near third extracellular loop. *Eur J Pharmacol* *403*, 37-44. 10.1016/s0014-2999(00)00578-1.
- Bowers, K.J., Chow, E., Xu, H., Dror, R.O., Eastwood, M.P., Gregersen, B.A., Klepeis, J.L., Kolossvary, I., Moraes, M.A., Sacerdoti, F.D., et al. (2006). Scalable Algorithms for Molecular Dynamics Simulations on Commodity Clusters. pp. 43.
- Branduardi, D., and Faraldo-Gómez, J.D. (2013). String method for calculation of minimum free-energy paths in Cartesian space in freely-tumbling systems. *Journal of chemical theory and computation* *9*, 4140-4154. 10.1021/ct400469w.
- Comer, S.D., and Cahill, C.M. (2019). Fentanyl: Receptor pharmacology, abuse potential, and implications for treatment. *Neurosci Biobehav Rev* *106*, 49-57. 10.1016/j.neubiorev.2018.12.005.

de Waal, P.W., Shi, J., You, E., Wang, X., Melcher, K., Jiang, Y., Xu, H.E., and Dickson, B.M. (2020). Molecular mechanisms of fentanyl mediated beta-arrestin biased signaling. *PLoS Comput Biol* *16*, e1007394. 10.1371/journal.pcbi.1007394.

Dijkstra, E.W. (1959). A note on two problems in connexion with graphs. *Numerische Mathematik* *1*, 269-271. 10.1007/BF01386390.

Dosen-Micovic, L., Ivanovic, M., and Micovic, V. (2006). Steric interactions and the activity of fentanyl analogs at the mu-opioid receptor. *Bioorganic & medicinal chemistry* *14*, 2887-2895. 10.1016/j.bmc.2005.12.010.

Dror, R.O., Arlow, D.H., Maragakis, P., Mildorf, T.J., Pan, A.C., Xu, H., Borhani, D.W., and Shaw, D.E. (2011). Activation mechanism of the beta2-adrenergic receptor. *Proc Natl Acad Sci U S A* *108*, 18684-18689. 10.1073/pnas.1110499108.

Ehrlich, A.T., Semache, M., Gross, F., Da Fonte, D.F., Runtz, L., Colley, C., Mezni, A., Le Gouill, C., Lukasheva, V., Hogue, M., et al. (2019). Biased Signaling of the Mu Opioid Receptor Revealed in Native Neurons. *iScience* *14*, 47-57. 10.1016/j.isci.2019.03.011.

Ellis, C.R., Kruhlak, N.L., Kim, M.T., Hawkins, E.G., and Stavitskaya, L. (2018). Predicting opioid receptor binding affinity of pharmacologically unclassified designer substances using molecular docking. *PLoS One* *13*, e0197734. 10.1371/journal.pone.0197734.

Gillis, A., Gondin, A.B., Kliewer, A., Sanchez, J., Lim, H.D., Alamein, C., Manandhar, P., Santiago, M., Fritzwanker, S., Schmiedel, F., et al. (2020). Low intrinsic efficacy for G protein activation can explain the improved side effect profiles of new opioid agonists. *Sci Signal* *13*. 10.1126/scisignal.aaz3140.

Haley, D.F., and Saitz, R. (2020). The Opioid Epidemic During the COVID-19 Pandemic. *JAMA* *324*, 1615-1617. 10.1001/jama.2020.18543.

Huang, W., Manglik, A., Venkatakrisnan, A.J., Laeremans, T., Feinberg, E.N., Sanborn, A.L., Kato, H.E., Livingston, K.E., Thorsen, T.S., Kling, R.C., et al. (2015). Structural insights into micro-opioid receptor activation. *Nature* 524, 315-321. 10.1038/nature14886.

Humphrey, W., Dalke, A., and Schulten, K. (1996). VMD: visual molecular dynamics. *J Mol Graph* 14, 33-38, 27-38.

Jin, W.Q., Xu, H., Zhu, Y.C., Fang, S.N., Xia, X.L., Huang, Z.M., Ge, B.L., and Chi, Z.Q. (1981). Studies on synthesis and relationship between analgesic activity and receptor affinity for 3-methyl fentanyl derivatives. *Sci Sin* 24, 710-720.

John, B., and Sali, A. (2003). Comparative protein structure modeling by iterative alignment, model building and model assessment. *Nucleic Acids Res* 31, 3982-3992.

Kapoor, A., Provasi, D., and Filizola, M. (2020). Atomic-Level Characterization of the Methadone-Stabilized Active Conformation of μ -Opioid Receptor. *Mol Pharmacol* 98, 475-486. 10.1124/mol.119.119339.

Kelly, E. (2013). Efficacy and ligand bias at the mu-opioid receptor. *Br J Pharmacol* 169, 1430-1446. 10.1111/bph.12222.

Koehl, A., Hu, H., Maeda, S., Zhang, Y., Qu, Q., Paggi, J.M., Latorraca, N.R., Hilger, D., Dawson, R., Matile, H., et al. (2018). Structure of the micro-opioid receptor-Gi protein complex. *Nature* 558, 547-552. 10.1038/s41586-018-0219-7.

Laio, A., and Parrinello, M. (2002). Escaping free-energy minima. *Proc Natl Acad Sci U S A* 99, 12562-12566. 10.1073/pnas.202427399.

Lalinde, N., Moliterni, J., Wright, D., Spencer, H.K., Ossipov, M.H., Spaulding, T.C., and Rudo, F.G. (1990). Synthesis and pharmacological evaluation of a series of new 3-methyl-1,4-disubstituted-piperidine analgesics. *J Med Chem* 33, 2876-2882. 10.1021/jm00172a032.

Lane, J.R., Abramyan, A.M., Adhikari, P., Keen, A.C., Lee, K.H., Sanchez, J., Verma, R.K., Lim, H.D., Yano, H., Javitch, J.A., and Shi, L. (2020). Distinct inactive conformations of the dopamine

D2 and D3 receptors correspond to different extents of inverse agonism. *Elife* 9.

10.7554/eLife.52189.

Li, J., Abel, R., Zhu, K., Cao, Y., Zhao, S., and Friesner, R.A. (2011). The VSGB 2.0 model: a next generation energy model for high resolution protein structure modeling. *Proteins* 79, 2794-2812. 10.1002/prot.23106.

Lipinski, P.F.J., Jaronczyk, M., Dobrowolski, J.C., and Sadlej, J. (2019). Molecular dynamics of fentanyl bound to mu-opioid receptor. *J Mol Model* 25, 144. 10.1007/s00894-019-3999-2.

Lu, C., Wu, C., Ghoreishi, D., Chen, W., Wang, L., Damm, W., Ross, G.A., Dahlgren, M.K., Russell, E., Von Bargen, C.D., et al. (2021). OPLS4: Improving Force Field Accuracy on Challenging Regimes of Chemical Space. *J Chem Theory Comput*. 10.1021/acs.jctc.1c00302.

Mafi, A., Kim, S.K., and Goddard, W.A., 3rd (2020). Mechanism of β -arrestin recruitment by the μ -opioid G protein-coupled receptor. *Proc Natl Acad Sci U S A* 117, 16346-16355.

10.1073/pnas.1918264117.

Maguire, P., Tsai, N., Kamal, J., Cometta-Morini, C., Upton, C., and Loew, G. (1992).

Pharmacological profiles of fentanyl analogs at mu, delta and kappa opiate receptors. *Eur J Pharmacol* 213, 219-225. 10.1016/0014-2999(92)90685-w.

Manglik, A., Kruse, A.C., Kobilka, T.S., Thian, F.S., Mathiesen, J.M., Sunahara, R.K., Pardo, L., Weis, W.I., Kobilka, B.K., and Granier, S. (2012). Crystal structure of the micro-opioid receptor bound to a morphinan antagonist. *Nature*. 10.1038/nature10954.

Mansour, A., Taylor, L.P., Fine, J.L., Thompson, R.C., Hoversten, M.T., Mosberg, H.I., Watson, S.J., and Akil, H. (1997). Key residues defining the mu-opioid receptor binding pocket: a site-directed mutagenesis study. *J Neurochem* 68, 344-353. 10.1046/j.1471-4159.1997.68010344.x.

Michino, M., Beuming, T., Donthamsetti, P., Newman, A.H., Javitch, J.A., and Shi, L. (2015). What can crystal structures of aminergic receptors tell us about designing subtype-selective ligands? *Pharmacol Rev* 67, 198-213. 10.1124/pr.114.009944.

Michino, M., Boateng, C.A., Donthamsetti, P., Yano, H., Bakare, O.M., Bonifazi, A., Ellenberger, M.P., Keck, T.M., Kumar, V., Zhu, C., et al. (2017). Toward Understanding the Structural Basis of Partial Agonism at the Dopamine D3 Receptor. *J Med Chem* *60*, 580-593. 10.1021/acs.jmedchem.6b01148.

Olsson, M.H., Sondergaard, C.R., Rostkowski, M., and Jensen, J.H. (2011). PROPKA3: Consistent Treatment of Internal and Surface Residues in Empirical pKa Predictions. *J Chem Theory Comput* *7*, 525-537. 10.1021/ct100578z.

Pándy-Szekeres, G., Munk, C., Tsonkov, T.M., Mordalski, S., Harpsøe, K., Hauser, A.S., Bojarski, A.J., and Gloriam, D.E. (2017). GPCRdb in 2018: adding GPCR structure models and ligands. *Nucleic Acids Research* *46*, D440-D446. 10.1093/nar/gkx1109.

Pasternak, G.W., and Pan, Y.X. (2013). Mu opioids and their receptors: evolution of a concept. *Pharmacol Rev* *65*, 1257-1317. 10.1124/pr.112.007138.

Podlewska, S., Bugno, R., Kudla, L., Bojarski, A.J., and Przewlocki, R. (2020). Molecular Modeling of μ Opioid Receptor Ligands with Various Functional Properties: PZM21, SR-17018, Morphine, and Fentanyl-Simulated Interaction Patterns Confronted with Experimental Data. *Molecules* *25*. 10.3390/molecules25204636.

Ricarte, A., Dalton, J.A.R., and Giraldo, J. (2021). Structural Assessment of Agonist Efficacy in the μ -Opioid Receptor: Morphine and Fentanyl Elicit Different Activation Patterns. *Journal of chemical information and modeling* *61*, 1251-1274. 10.1021/acs.jcim.0c00890.

Roos, K., Wu, C., Damm, W., Reboul, M., Stevenson, J.M., Lu, C., Dahlgren, M.K., Mondal, S., Chen, W., Wang, L., et al. (2019). OPLS3e: Extending Force Field Coverage for Drug-Like Small Molecules. *J Chem Theory Comput* *15*, 1863-1874. 10.1021/acs.jctc.8b01026.

Schmid, C.L., Kennedy, N.M., Ross, N.C., Lovell, K.M., Yue, Z., Morgenweck, J., Cameron, M.D., Bannister, T.D., and Bohn, L.M. (2017). Bias Factor and Therapeutic Window Correlate to Predict Safer Opioid Analgesics. *Cell* *171*, 1165-1175 e1113. 10.1016/j.cell.2017.10.035.

Sherman, W., Day, T., Jacobson, M.P., Friesner, R.A., and Farid, R. (2006). Novel procedure for modeling ligand/receptor induced fit effects. *J Med Chem* 49, 534-553. 10.1021/jm050540c.

Spivak, C.E., Beglan, C.L., Seidleck, B.K., Hirshbein, L.D., Blaschak, C.J., Uhl, G.R., and Surratt, C.K. (1997). Naloxone activation of mu-opioid receptors mutated at a histidine residue lining the opioid binding cavity. *Mol Pharmacol* 52, 983-992. 10.1124/mol.52.6.983.

Stahl, E.L., and Bohn, L.M. (2021). Low Intrinsic Efficacy Alone Cannot Explain the Improved Side Effect Profiles of New Opioid Agonists. *Biochemistry*. 10.1021/acs.biochem.1c00466.

Stanley, T.H. (2014). The fentanyl story. *J Pain* 15, 1215-1226. 10.1016/j.jpain.2014.08.010.

Stolzenberg, S., Michino, M., LeVine, M.V., Weinstein, H., and Shi, L. (2016). Computational approaches to detect allosteric pathways in transmembrane molecular machines. *Biochim Biophys Acta* 1858, 1652-1662. 10.1016/j.bbamem.2016.01.010.

Subramanian, G., Paterlini, M.G., Portoghese, P.S., and Ferguson, D.M. (2000). Molecular docking reveals a novel binding site model for fentanyl at the mu-opioid receptor. *J Med Chem* 43, 381-391. 10.1021/jm9903702.

The Drug Enforcement Administration's (DEA) Special Testing and Research Laboratory's Emerging Trends Program. DEA Emerging Threat Reports.
<https://ndews.umd.edu/resources/dea-emerging-threat-reports>.

Van Bever, W.F., Niemegeers, C.J., and Janssen, P.A. (1974). Synthetic analgesics. Synthesis and pharmacology of the diastereoisomers of N-(3-methyl-1-(2-phenylethyl)-4-piperidyl)-N-phenylpropanamide and N-(3-methyl-1-(1-methyl-2-phenylethyl)-4-piperidyl)-N-phenylpropanamide. *J Med Chem* 17, 1047-1051. 10.1021/jm00256a003.

Vo, Q.N., Mahinthichaichan, P., Shen, J., and Ellis, C.R. (2021). How mu-opioid receptor recognizes fentanyl. *Nat Commun* 12, 984. 10.1038/s41467-021-21262-9.

Wax, P.M., Becker, C.E., and Curry, S.C. (2003). Unexpected "gas" casualties in Moscow: a medical toxicology perspective. *Ann Emerg Med* 41, 700-705. 10.1067/mem.2003.148.

Xu, H., Kim, C.H., Zhu, Y.C., Weber, R.J., Jacobson, A.E., Rice, K.C., and Rothman, R.B. (1991). (+)-cis-3-methylfentanyl and its analogs bind pseudoirreversibly to the mu opioid binding site: evidence for pseudoallosteric modulation. *Neuropharmacology* 30, 455-462. 10.1016/0028-3908(91)90006-w.

Xu, H., Lu, Y.F., Partilla, J.S., Zheng, Q.X., Wang, J.B., Brine, G.A., Carroll, F.I., Rice, K.C., Chen, K.X., Chi, Z.Q., and Rothman, R.B. (1999). Opioid peptide receptor studies, 11: involvement of Tyr148, Trp318 and His319 of the rat mu-opioid receptor in binding of mu-selective ligands. *Synapse* 32, 23-28. 10.1002/(SICI)1098-2396(199904)32:1<23::AID-SYN3>3.0.CO;2-N.

Yeadon, M., and Kitchen, I. (1988). Differences in the characteristics of opioid receptor binding in the rat and marmoset. *J Pharm Pharmacol* 40, 736-739. 10.1111/j.2042-7158.1988.tb07008.x.

Zawilska, J.B., Kuczynska, K., Kosmal, W., Markiewicz, K., and Adamowicz, P. (2021). Carfentanil - from an animal anesthetic to a deadly illicit drug. *Forensic Sci Int* 320, 110715. 10.1016/j.forsciint.2021.110715.